Published OnlineFirst July 15, 2020; DOI: 10.1158/1535-7163.MCT-19-1004

ARX788, a Site-specific Anti-HER2 Antibody–Drug Conjugate, Demonstrates Potent and Selective Activity in HER2-low and T-DM1–resistant Breast and Gastric Cancers

Lillian Skidmore, Sukumar Sakamuri, Nick A. Knudsen, Amha Gebre Hewet, Snezana Milutinovic, Wisam Barkho, Sandra Lyn Biroc, Jessica Kirtley, Robin Marsden, Kristine Storey, Ianina Lopez, Wayne Yu, Shiao-Yan Fang, Sulan Yao, Yi Gu, and Feng Tian

ABSTRACT

First-generation antibody–drug conjugates (ADC) are heterogeneous mixtures that have shown clinical benefit, but generally exhibited safety issues and a narrow therapeutic window due, in part, to off-target toxicity caused by ADC instability. ARX788 is a next-generation, site-specific anti-HER2 ADC that utilizes a unique nonnatural amino acid–enabled conjugation technology and a noncleavable Amberstatin (AS269) drug-linker to generate a homogeneous ADC with a drug-to-antibody ratio of 1.9. ARX788 exhibits high serum stability in mice and a relatively long ADC half-life of 12.5 days. When compared *in vitro* against T-DM1 across a panel of cancer cell lines, ARX788 showed superior activity in the lower HER2-expressing cell lines and no activity in normal cardiomyocyte cells. Similarly, ARX788 significantly inhibited tumor growth, and generally outperformed T-DM1 in HER2-high and HER2-low expression xenograft models. Breast and gastric cancer patient-derived xenograft studies confirmed strong antitumor activity of ARX788 in HER2-positive and HER2-low expression tumors, as well as in a T-DM1-resistant model. The encouraging preclinical data support the further development of ARX788 for treatment of patients with HER2-positive breast and gastric cancer, including those who have developed T-DM1 resistance, and patients with HER2-low expression tumors who are currently ineligible to receive HER2-targeted therapy.

Introduction

After a prolonged development period, the antibody–drug conjugate (ADC) field has finally progressed from the initial concept of antibody-guided delivery of cytotoxic payloads to the regulatory approval (or accelerated approval) of seven ADC therapeutics, brentuximab vedotin (Adcetris), ado-trastuzumab emtansine (T-DM1), gemtuzumab ozogamicin (Mylotarg), inotuzumab ozogamicin (Besponsa), polatuzumab vedotin-piiq (Polivy), enfortumab vedotin (Padcev), and trastuzumab deruxtecan (Enhertu) (1–7). This first-generation of ADCs has demonstrated clinical benefit, spurring companies to develop next-generation ADCs to further improve ADC stability and safety, and thus widen the therapeutic window.

Generally, the mechanism of ADCs relies on the antibody binding to a specific target expressed on the tumor cell surface, internalization of the ADC, proteolytic degradation of the antibody and/or linker, and release of the payload in the lysosome of the cell. The payload then diffuses into the cytoplasm or nucleus to exert its cytotoxic effects. In the case of auristatin payloads, destabilization of microtubules (8) leads to cell-cycle arrest and subsequent tumor cell apoptosis (9, 10).

Optimization of each ADC component, antibody, conjugation site, conjugation chemistry, linker, and drug, can improve pharmacokinetics, efficacy, and safety (11–15). First-generation ADCs utilized random, uncontrolled conjugation of drug-linker to surface-exposed cysteine or lysine residues, which resulted in heterogeneous ADC mixtures with high average drug-to-antibody ratio (DAR) values. In recent years, companies in the ADC field have reported on the advantages of site-specific conjugation over random conjugation, showing a DAR of two can be superior to higher DAR ADCs due to less aggregation, slower systemic clearance, higher activity, and less toxicity (16–20).

We have developed a unique, clinically validated conjugation technology in which drugs are site specifically attached to an antibody via a stable oxime bond formed by conjugating a hydroxylamine containing drug-linker with a nonnatural amino acid, *para*-acetylphenylalanine (pAF), incorporated into an antibody. This results in precisely two drug-linkers conjugated site specifically to one antibody. pAF can be incorporated into most surface-exposed sites of an antibody for screening optimal conjugation sites, an advantage compared with other site-specific conjugation technologies, in which reportedly only a limited number of sites in the antibody are amenable to conjugation (21–23).

Herein, we describe the preclinical characterization of a next-generation, site-specific anti-HER2 ADC, ARX788, comprised of a humanized HER2 targeting mAb conjugated to a cytotoxic tubulin inhibitor, Amberstatin (AS269), using Ambrx's nonnatural amino acid incorporation technology platform. ARX788 is homogeneous and highly stable, which can lead to a wider therapeutic window by delivering drug to target tumor cells with higher efficiency, thus maximizing on-target efficacy and minimizing off-target toxicity.

Ambrx, Inc, La Jolla, California.

Note: Supplementary data for this article are available at Molecular Cancer Therapeutics Online (http://mct.aacrjournals.org/).

Corresponding Author: Feng Tian, Ambrx, 10975 North Torrey Pines Rd, La Jolla, CA 92037. Phone: 858-875-2473; E-mail: feng.tian@ambrx.com

Mol Cancer Ther 2020;19:1833–43

doi: 10.1158/1535-7163.MCT-19-1004

Published OnlineFirst July 15, 2020; DOI: 10.1158/1535-7163.MCT-19-1004

Materials and Methods

Site-specific ADC conjugation

pAF containing anti-HER2 antibody was concentrated to 10–20 mg/mL in conjugation buffer (30 mmol/L sodium acetate, pH 4.0). Acetic hydrazide and 10 molar equivalents of hydroxyl-amine functionalized AS269 drug-linker were added to the antibody. The conjugation reaction was continued for 18–20 hours at 30°C followed by purification over a Capto SP Impres Column (GE Healthcare) to remove excess reagents. The purified ADC was buffer exchanged into formulation buffer and stored at ≤65°C until further use.

Reversed-phase high-performance liquid chromatography

mAb and ADC samples were analyzed on a ZORBAX StableBond C3 Column (Agilent Technologies, catalog no.: 863973-909) using an Agilent 1100 HPLC System with UV detection at 214 nm. The column was first equilibrated at 70% mobile phase A (0.1% TFA in water) and 30% mobile phase B (0.1% TFA in acetonitrile) for 1 minute, followed by a linear gradient from 30% B to 50% B over 20 minutes where the analyte eluted. The column was kept at 75°C and flow rate was maintained at 1 mL/minute. For reduced samples, mAb and ADC were treated with 20 mmol/L dithiothreitol in 6 mol/L guanidine-HCl and 50 mmol/L TRIS-HCl, pH 7.8 at 56°C for 30 minutes prior to high-performance liquid chromatography (HPLC) analysis. Nonreduced and reduced samples were injected at 7 μg per load. On the basis of the nonreduced ADC chromatogram, percent areas of DAR 0, 1, and 2 species were quantified using Agilent ChemStation Software, and DAR was calculated using the following equation: DAR = (% area of DAR1 + % area of DAR2 × 2)/100.

Size exclusion-HPLC

mAb and ADC samples were analyzed on a TSKgel G3000SW$_{XL}$ Column (Tosoh Bioscience, catalog no.: 08541) using an Agilent 1100 HPLC System with UV detection at 280 nm. Samples were injected at 50 μg load. Separation was achieved by isocratic elution using a mobile phase consisting of 200 mmol/L potassium phosphate, 250 mmol/L potassium chloride, pH 6.0 at a flow rate of 0.5 mL/minute and column temperature set at 25°C. Percent area of high molecular weight (HMW), monomer, and low molecular weight species was calculated using Agilent ChemStation Software.

In Vitro tubulin polymerization assay

A cell-free tubulin polymerization assay was performed according to the manufacturer's instructions (Cytoskeleton, catalog no.: BK011P). Briefly, serially diluted samples were added to a 96-well half-area plate prewarmed at 37°C. Tubulin master mix was then added to the samples, and plates were analyzed in a fluorometer set to 37°C with readings every 60 seconds for 60 minutes. Mean slope values for each sample were calculated with Tecan Magellan Software, and IC_{50} values were determined with a four-parameter regression model.

HER2 binding affinity

HER2 multi-concentration binding kinetic experiments were performed on an Octet RED96 instrument at 30°C. Anti-human Fc Capture Biosensors (PALL/ForteBio, catalog no.: 18-5063) were loaded with anti-HER2 mAb or ARX788 until levels reached 1.3–1.7 nmol/L and then washed with 1X HBS-P+ Buffer (GE Healthcare) to remove unbound protein. For association phase monitoring, HER2 was diluted to concentrations ranging from 1.25 to 100 nmol/L and allowed to bind loaded biosensors for 180 seconds. The dissociation phase was recorded in wells containing 1X HBS-P+ buffer for 300 seconds. Data were referenced using a parallel buffer blank subtraction, and the baseline was aligned to the *y*-axis and smoothed by a Savitzky–Golay filter in the Octet data analysis software. The processed kinetic sensorgrams were globally fitted using the Langmuir model describing a 1:1 binding stoichiometry.

Fc receptor binding affinity

Multi-concentration binding kinetic experiments were performed on an Octet RED96 instrument at 30°C. 1X HBS-P+ Buffer (GE Healthcare) was used for CD64, CD32a, and CD16a binding assays. Sodium phosphate (100 mmol/L), 150 mmol/L sodium chloride, and 0.05% (v/v) Tween 20, pH 6.0 buffer was used for FcRn binding assays. Biotinylated human Fc receptors (CD64, CD32a, CD16a, and FcRn) were immobilized on Streptavidin-coated Biosensors (PALL/ForteBio, 18–5019) until levels between 0.1 and 0.5 nm were reached. The loaded biosensors were washed with the appropriate assay buffer (described above) for 60 seconds to remove any unbound protein. For association phase monitoring, anti-HER2 mAb and ARX788 samples were diluted to concentrations ranging between 2.5 and 1,000 nmol/L and allowed to bind loaded biosensors for 30–180 seconds. The dissociation phase was recorded in wells containing assay buffer for 100–1,000 seconds. Data were referenced using a parallel buffer blank subtraction, and the baseline was aligned to the *y*-axis and smoothed by a Savitzky–Golay filter in the Octet data analysis software. Processed binding curves were globally fitted using the Langmuir model describing a 1:1 binding stoichiometry.

In Vitro cell proliferation and HER2 receptor quantification

Human breast cancer (SK-BR-3 RRID:CVCL_0033, HCC1954 RRID:CVCL_1259, BT-474 RRID:CVCL_0179, MDA-MB-453 RRID:CVCL_0418, MDA-MB-175 RRID:CVCL_1400, MCF-7 RRID:CVCL_0031, MDA-MB-231 RRID:CVCL_0062, and MDA-MB-468 RRID:CVCL_0419), lung cancer (Calu-3 RRID:CVCL_0609), ovarian cancer (SKOV-3 RRID:CVCL_0532 and OVCAR-3 RRID:CVCL_0465), gastric cancer (NCI-N87 RRID:CVCL_1603), and normal cardiomyocyte (AC-10 RRID:CVCL_4U16) cell lines were purchased from ATCC. The breast cancer cell line, JIMT-1 (RRID:CVCL_2077), was purchased from AddexBio (catalog no.: C0006005). All *in vitro* experiments were conducted with cells passaged for fewer than 3 months after original vial thaw, so cell line authentication testing was not conducted. Cells were harvested and seeded at optimized densities in the manufacturer-recommended assay medium to white, 96-well plates. The following day, serially diluted ARX788 or T-DM1 was added to the plated cells and incubated for approximately 72 hours in an incubator set to 37°C and 5% CO_2. CellTiter Glo 2.0 (Promega, catalog no.: G9241) was then added to measure cell viability. IC_{50} values were determined with a four-parameter regression model in GraphPad Prism.

HER2 cell surface receptor number was quantified using QiFiKit (Dako, catalog no.: K0078). Cell lines were harvested and stained with mouse anti-HER2 antibody (BioLegend, Clone 24D2) for 1 hour at 4°C. After washing, cells and QiFiKit control beads were stained with anti-mouse IgG-FITC secondary antibody for 45 minutes at 4°C, washed twice, and analyzed on a flow cytometer in the FITC channel. HER2 receptor number per cell was calculated on the basis of the reference curve generated with the QiFiKit control beads.

MDA-MB-435 HER2 pool generation

A total of 20×10^6 MDA-MB-435 cells transduced with *HER2* (kind gift from Calibr, La Jolla, CA) were stained with anti-HER2-PE

Published OnlineFirst July 15, 2020; DOI: 10.1158/1535-7163.MCT-19-1004

(BioLegend, catalog no.: 324406), washed, resuspended in 2 mL PBS + 2% FBS, and then sorted into pools with low, medium, and high expression levels. After expanding pools for 9 days, the parental cells and HER2 pools were quantified for HER2 expression by QiFiKit analysis (see previous description). Cells were seeded at 1,000 cells per well and treated with ARX788 for 3 days, after which cell viability was determined with CellTiter Glo 2.0. IC_{50} values were determined with a four-parameter regression model in GraphPad Prism.

All *in vivo* studies were approved by the local animal care and use committees and conducted in accordance with established guidelines.

Pharmacokinetic studies

Twenty male nude mice (Charles River Laboratories) were dosed once intravenously with 3 mg/kg ARX788 or unconjugated mAb ($n = 10$ mice/group). Whole-blood samples were collected from 4 animals at each timepoint, immediately diluted in Casein Blocker (Thermo Fisher Scientific), and frozen at −70°C prior to analysis. The Format 1 total antibody assay uses recombinant human ErbB2/HER2-Fc Chimera Protein (R&D Systems, catalog no.: 1129-ER-050) as capture antigen, and detects with biotinylated goat anti-human kappa light chain (Southern Biotech, catalog no.: 2060-08) and Streptavidin SULFO-TAG (Meso Scale Discovery, catalog no.: R32AD-1). The Format 3 intact ADC assay quantifies DAR2 ADCs by using a proprietary anti-AS269 antibody (AMB-20) as capture antibody, and biotinylated AMB-20 and streptavidin SULFO-TAG for detection. For both formats, addition of 1× MSD Read Buffer and application of an electrical current by the MSD Sector Imager 2400 produces an electrochemiluminescent signal expressed in relative light units (RLU). The conversion of RLU to concentration was achieved using a four-parameter regression model with $1/Y^2$ weighing in the MSD Workbench Software. Pharmacokinetic parameters were calculated using a noncompartmental model in WinNonlin (Certara) and reported as mean ± SD.

Cell line–derived xenograft models

The JIMT-1 xenograft study was conducted at Charles River Piedmont Research Center. Female CB17.SCID mice, 8–12 weeks of age, were inoculated subcutaneously in the right flank with 10×10^6 JIMT-1 cells in 50% Matrigel. When tumors reached 100–150 mm^3 in size, mice were randomized into groups of 8 animals and dosed intravenously with vehicle or ADCs.

The BT474-EEI and NCI-N87 xenograft studies were performed at Ambrx. BT474 tumors were serially passaged in mice for six passages with decreasing amounts of estrogen pellets, and in the last few passages, no exogenous estrogen was present. Fragments of the fastest growing tumors were implanted subcutaneously into the right flank of female SCID-beige mice (Charles River Laboratories), 4–5 weeks of age. When tumors reached approximately 100–300 mm^3 in size, mice were randomized into groups of 9 animals and dosed twice (21 days apart) intravenously with vehicle or ADCs. For the NCI-N87 model, female nude mice (Charles River Laboratories), 5–6 weeks of age, were inoculated subcutaneously in the right flank with 10×10^6 NCI-N87 cells in 50% Matrigel. When tumors reached approximately 200–400 mm^3 in size, mice were randomized into groups of 10 animals and dosed intravenously with vehicle or ADCs.

Charles River MAX1162F and XenTech T226 patient-derived xenograft models

Female athymic nude mice, 4–6 weeks of age, were implanted subcutaneously with tumor fragments passaged in donor mice. Prior to implantation, tumors were tested by IHC for verification of HER2 IHC3+ status. Animals with tumors 50–200 mm^3 in size were randomized into groups of 10 mice and injected intravenously with ARX788, T-DM1, or vehicle.

GenenDesign breast and gastric patient-derived xenograft models

Female nude mice, 6–9 weeks of age, were implanted subcutaneously with tumor fragments 15–30 mm^3 in size in the right flank. Once tumors reached 100–200 mm^3, mice were randomized into groups of 8 animals and injected intravenously with ARX788 or vehicle. Prior to implantation, tumors were tested by IHC and FISH for verification of HER2 status.

For the above studies, animals were weighed, and tumors were measured by caliper, once or twice weekly. Tumor volumes (TV) were calculated using the formula: TV (mm^3) = [length (mm) × width $(mm)^2$] × 0.5, in which length and width are the longest and the shortest diameters of the tumor, respectively. Treated versus control (T/C) was calculated by dividing the mean final tumor volume of treated group by the mean final tumor volume of control group. Percent tumor growth inhibition (% TGI) was calculated by the following formula: % TGI = [1 − T/C] × 100. A % TGI value > 80% was considered tumor regression.

Statistical analysis

Statistical significance between treated and control groups was evaluated in GraphPad Prism version 7.0 using two-way ANOVA with repeated measures and Bonferroni post-test. A $P < 0.05$ was considered statistically significant.

IHC and FISH analysis

GenenDesign patient-derived xenograft (PDX) tumor samples were stained for HER2 expression by IHC at Reveal Biosciences with an optimized method using rabbit anti-HER2 antibody (Cell Signaling Technology, catalog no.: 2165). In addition, FISH staining with a dual-color HER2/CEP17 FISH Kit (GP Medical Co) was conducted to verify *HER2* amplification in the PDX samples. Board-certified pathologists scored the HER2 protein expression and gene-copy number. The Charles River MAX1162F PDX tumor samples were verified for HER2 expression by IHC using DAKO anti-HER2 antibody (catalog no.: A0485). Histalim confirmed HER2 expression in XenTech T226 PDX tumors by HER2 IHC staining.

Results

AS269 drug-linker design and activity

To maximize linker stability, we designed Amberstatin drug-linker (AS269) with a short, noncleavable hydroxylamine-PEG4 linker attached to the *N*-terminus of monomethyl auristatin F (MMAF; **Fig. 1A**). MMAF is a highly potent synthetic auristatin derivative that inhibits cellular proliferation by disrupting tubulin polymerization (9). MMAF and AS269 are relatively membrane impermeable, with poor activity observed in cellular proliferation assays.

Activity of MMAF and AS269 was measured in a cell-free tubulin polymerization assay to assess whether attachment of the PEG4 linker impacted activity. Both MMAF and AS269 inhibited tubulin polymerization similarly (**Fig. 1B**; $IC_{50} = 0.7$ μmol/L), confirming attachment of the PEG linker at the *N*-terminus of MMAF did not impair AS269 activity. MMAF and AS269 were approximately 2-fold more potent than positive control dolastatin, while a negative control drug (AXC-273) showed minimal activity in the tubulin polymerization assay.

Published OnlineFirst July 15, 2020; DOI: 10.1158/1535-7163.MCT-19-1004

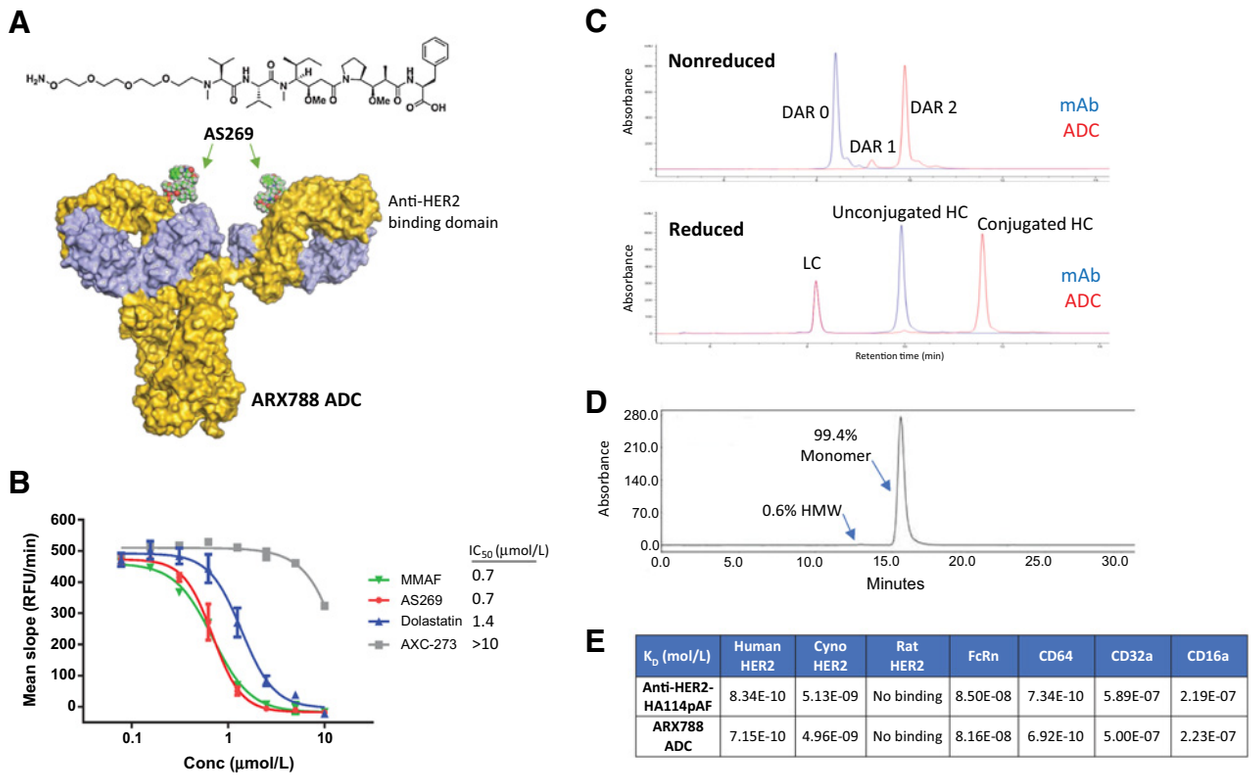

K_D (mol/L)	Human HER2	Cyno HER2	Rat HER2	FcRn	CD64	CD32a	CD16a
Anti-HER2-HA114pAF	8.34E-10	5.13E-09	No binding	8.50E-08	7.34E-10	5.89E-07	2.19E-07
ARX788 ADC	7.15E-10	4.96E-09	No binding	8.16E-08	6.92E-10	5.00E-07	2.23E-07

Figure 1.

Structure and characterization of Amberstatin AS269 drug-linker and ARX788. **A,** Chemical structure of AS269 drug-linker, which was site specifically conjugated to the heavy chain Ala114 of anti-HER2 mAb to generate ARX788. **B,** Activity of MMAF, AS269, dolastatin, and negative control AXC-273 (IC_{50} values listed) in a cell-free tubulin polymerization assay. **C,** Nonreduced and reduced RP-HPLC chromatograms of unconjugated mAb or ARX788 to determine DAR and location of drug-linker conjugation. **D,** SE-HPLC chromatogram of ARX788 with main peak and HMW species shown. **E,** Binding affinity of unconjugated mAb and ARX788 against human, cynomolgus (cyno), rat HER2; FcRn; CD64; CD32a; and CD16a as measured by Octet.

Site-specific conjugation results in monomeric ADCs with DAR 1.9

AS269 was site specifically conjugated to the pAF incorporated into an anti-HER2 antibody (Supplementary Fig. S1) at the heavy chain alanine 121 position, which corresponds to alanine 114 (HA114) by Kabat numbering, to generate ARX788 (**Fig. 1A**). In a nonreduced reversed-phase (RP)-HPLC method, ARX788 resolved primarily as a DAR2 species with a DAR value of 1.9. The reduced RP-HPLC profiles showed no change to the light chain peak, but a clear shift of the heavy chain peak after conjugation, confirming AS269 conjugated only to the heavy chain (**Fig. 1C**). In size exclusion (SE)-HPLC chromatograms, ARX788 aggregation was minimal with 99.4% monomer and 0.6% HMW species (**Fig. 1D**).

AS269 conjugation at site HA114 does not impact antibody binding

The binding affinities of anti-HER2 antibody and ARX788 to human, cynomolgus, and rat HER2 were determined by Octet analysis. The mAb and ARX788 both showed similar binding affinity (K_d values within 1.2-fold) to human and cynomolgus *HER2*, and no binding to rat HER2 (**Fig. 1E**). Thus, conjugation of AS269 at position HA114 did not impair the ability of ARX788 to bind HER2 antigen across multiple species. Additional characterization studies showed no difference in binding affinity of ARX788 and anti-HER2 antibody for FcRn, or the Fc gamma receptors CD64, CD32a, and CD16a (**Fig. 1E**).

ARX788 demonstrates superior *in vitro* activity compared with T-DM1

The *in vitro* activity of ARX788 and T-DM1 was evaluated across a panel of breast, gastric, lung, and ovarian cancer cell lines that expressed varying levels of HER2. Normal AC10 cardiomyocytes were also evaluated. HER2 cell surface receptor number was quantified using QiFiKit for all cell lines, and the expression ranged from 0 to 1,132,000 receptors per cell (**Table 1**). On the basis of commercially approved kits and reports in literature, the HER2 IHC and FISH scores for cell lines are also listed in **Table 1**.

ARX788 showed activity (sub-nmol/L potency or >50% efficacy) in cancer cell lines with ≥60,000 or 100,000 HER2 receptors (a potential threshold for ARX788 activity) and generally exhibited higher potency or maximum efficacy as HER2 expression increased. The QiFiKit HER2 receptor quantification levels correlated well with reported IHC and FISH scores, and ARX788 inhibited proliferation of cells classified as HER2 IHC3+, IHC2+, and IHC1+.

ARX788 was inactive in cancer cells expressing ≤46,000 HER2 receptors and in AC10 normal cardiomyocytes, which expressed 13,000 HER2 receptors. Thus, a significant difference in HER2 expression was observed in normal cells versus tumor cells that responded to

Published OnlineFirst July 15, 2020; DOI: 10.1158/1535-7163.MCT-19-1004

Table 1. Comparison of ARX788 and T-DM1 *in vitro* activity in cell lines with variable HER2 expression.

			ARX788		T-DM1		ARX788 potency gain (fold)	HER2 IHC/FISH reports	
Cell line	Tissue	HER2 cell surface number	IC_{50} (nmol/L)	Maximum efficacy (%)	IC_{50} (nmol/L)	Maximum efficacy (%)		HER2 IHC[a,b,c]	*HER2* amplification (FISH)[d,e]
SK-BR-3	Breast cancer	1,132,000	0.025	77	0.057	72	2.3	3+	Positive
HCC1954	Breast cancer	911,000	0.049	71	0.075	67	1.5	NR	NR
Calu-3	Lung cancer	900,000	0.316	49	1.22	40	3.9	NR	NR
BT-474	Breast cancer	821,000	0.250	63	2.01	46	8.0	3+	NR
NCI-N87	Gastric cancer	750,000	0.098	68	0.130	69	1.3	3+	NR
SKOV-3	Ovarian cancer	645,000	0.061	52	0.059	55	1.0	3+	NR
MDA-MB-453	Breast cancer	117,000	0.137	33	4.16	65	30	2+	Positive
JIMT-1	Breast cancer	106,000	0.097	65	14.9	81	154	2+	NR
MDA-MB-175	Breast cancer	62,000	0.246	40	2.15	39	8.7	1+	Negative
OVCAR-3	Ovarian cancer	46,000	No activity (>30 nmol/L)	19	~30	52	NA	NR	NR
MCF-7	Breast cancer	21,000	No activity (>30 nmol/L)	0	No activity (>30 nmol/L)	0	NA	0	NR
AC10	Normal cardiomyocytes	13,000	No activity (>30 nmol/L)	7	No activity (>30 nmol/L)	17	NA	NR	NR
MDA-MB-231	Breast cancer	12,000	No activity (>30 nmol/L)	0	ND	ND	NA	0	Negative
MDA-MB-468	Breast cancer	0	No activity (>100 nmol/L)	2	21	76	NA	0	NR

Abbreviations: NA, not applicable; ND, not determined; NR, not reported.
[a]Dako HercepTest IHC.
[b]VENTANA anti-HER2 (4B5) IHC.
[c]Li and colleagues (12).
[d]Bartlett JMS, Ibrahim M, Jasani B, Morgan JM, Ellis I, Kay E, et al. External quality assurance of HER2 FISH and ISH testing: three years of the UK National External Quality Assurance Scheme. Am J Clin Pathol 2009;131:106–111.
[e]PathVysion HER-2 DNA Probe kit.

ARX788 treatment. The ARX788-insensitive MCF-7, MDA-MB-231, and MDA-MB-468 cells expressed ≤20,000 HER2 receptors and are classified as IHC0 in literature, whereas the ARX788-sensitive MDA-MB-175 cells (62,000 HER2 receptors) are defined as IHC1+. In this limited dataset, current IHC methods can potentially identify patients with breast cancer expressing enough HER2 receptor to respond to ARX788 treatment.

When directly compared against T-DM1, ARX788 showed comparable or higher activity in high HER2 expressors, and superior activity in low HER2 expressors. In cell lines JIMT-1, MDA-MB-453, and MDA-MB-175, ARX788 was more potent than T-DM1 by a factor of 154×, 30×, and 9×, respectively (**Table 1**). These cell lines are reportedly HER2 IHC2+ or 1+, suggesting ARX788 activity may more significantly differentiate from T-DM1 in tumors with lower HER2 expression levels.

Importantly, ARX788 activity was antigen dependent as activity in a HER2-negative cell line (MDA-MB-468) was not observed. However, at higher concentrations of T-DM1, nonspecific inhibition of MDA-MB-468 cell proliferation was observed (IC_{50} = 21 nmol/L; efficacy = 76%). To further confirm the activity of ARX788 was dependent on HER2 expression, MDA-MB-435 melanoma cells were transduced with *HER2* and sorted into low-, medium-, and high-expressing pools. HER2 receptor expression levels for the parental MDA-MB-435 cell line and the three pools were confirmed by QiFiKit analysis, and all cells were incubated with ARX788 to evaluate activity (Supplementary Fig. S2). ARX788 showed no activity in the parental cell line (8,000 receptors), moderate activity in the HER2-low pool (137,000 receptors), and strong activity in the HER2-medium (384,000 receptors) and HER2-high (821,000 receptors) pools. These data in isogenic cells provided additional evidence for HER2 as a reliable biomarker of ARX788 activity.

ARX788 exhibits stability in circulation and enhanced pharmacokinetics

Ambrx site-specific conjugation technology precisely generated ADCs with two drugs per antibody. By comparing the intact ADC (detects DAR2 ADC only) and total antibody (detects all unconjugated and conjugated antibodies) curves, loss of a single drug-linker can be detected and ADC stability stringently monitored. To determine ARX788 stability in circulation and pharmacokinetic parameters, nude mice (n = 10 animals/group) were injected with 3 mg/kg ARX788 or unconjugated anti-HER2 antibody, and collected blood samples were analyzed in the Format 1 total antibody assay and the Format 3 intact ADC assay (**Fig. 2A**). The ARX788 total antibody and intact ADC concentration–time curves overlapped completely, demonstrating ARX788 was highly stable in circulation and remained intact as a DAR2 ADC throughout the 18-day study (**Fig. 2B**). In addition, the anti-HER2 mAb and ARX788 Format 1 concentration–time curves were very similar with comparable clearance (0.79 and 0.49 mL/hour/kg, respectively), exposure (AUC 4,100,000 and 6,300,000 hr*ng/mL, respectively), and half-life (257 and 299 hours, respectively; **Fig. 2B**).

ARX788 shows stronger antitumor activity than T-DM1 in cell line–derived xenograft models

ARX788 and T-DM1 were evaluated in xenograft models using cell lines with higher (BT474-EEI and NCI-N87) or lower (JIMT-1) HER2 expression. In the breast cancer BT474-EEI xenograft model, mice (n = 9/group) were treated with two doses of 1 or 3 mg/kg ARX788,

Published OnlineFirst July 15, 2020; DOI: 10.1158/1535-7163.MCT-19-1004

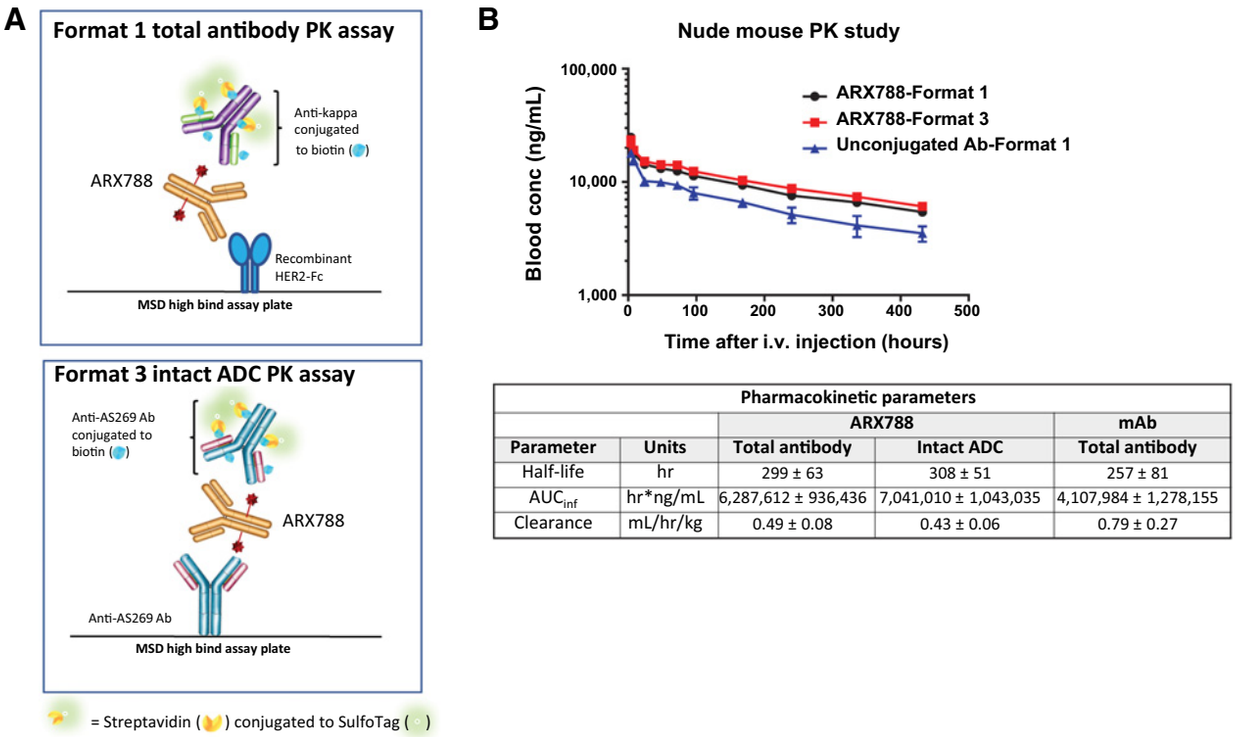

Pharmacokinetic parameters				
		ARX788		mAb
Parameter	Units	Total antibody	Intact ADC	Total antibody
Half-life	hr	299 ± 63	308 ± 51	257 ± 81
AUC_{inf}	hr*ng/mL	6,287,612 ± 936,436	7,041,010 ± 1,043,035	4,107,984 ± 1,278,155
Clearance	mL/hr/kg	0.49 ± 0.08	0.43 ± 0.06	0.79 ± 0.27

Figure 2.

Pharmacokinetic (PK) study of ARX788 in mice. **A,** Format 1 total antibody and Format 3 intact ADC ligand-binding pharmacokinetic assay formats. **B,** Nude mice (n = 10/group) received a single 3 mg/kg intravenous (i.v.) dose of unconjugated mAb or ARX788, and blood samples were collected and tested in the total antibody and intact ADC assays. Overlay of the concentration–time curves for the ARX788 samples quantified in total antibody and intact ADC assays, and the unconjugated mAb samples in the total antibody assay. Pharmacokinetic parameters were calculated using WinNonlin noncompartmental analysis and reported as mean values ± SD.

T-DM1, or vehicle. ARX788 dose dependently regressed tumors, whereas equivalent doses of T-DM1 resulted in less TGI (**Fig. 3A**). The antitumor activity of 3 mg/kg T-DM1 was similar to that of 1 mg/kg ARX788. At study end, ARX788 treatment led to 6 of 9 or 8 of 9 mice with no measurable tumor at the 1 or 3 mg/kg doses, respectively, whereas T-DM1 at 1 or 3 mg/kg doses resulted in 1 of 9 or 6 of 9 animals with no measurable tumor, respectively.

In the gastric NCI-N87 xenograft model (**Fig. 3B**), a single 1 or 5 mg/kg dose of ARX788 significantly inhibited tumor growth with TGI = 39% and 90%, respectively. Treatment with corresponding doses of T-DM1 resulted in significantly less TGI. An isotype control-AS269 ADC dosed at 5 mg/kg resulted in no TGI, confirming ARX788 activity is mediated by HER2 binding.

In the JIMT-1 breast cancer xenograft model, which expressed lower levels of HER2, a single 1 or 3.3 mg/kg dose of ARX788 showed strong dose-dependent TGI, with tumors eradicated at the higher dose (**Fig. 3C**). However, a single 3.3 mg/kg dose of T-DM1 or isotype control-AS269 ADC was completely ineffective in this model, confirming superior activity of ARX788 versus T-DM1 in a HER2-low expression xenograft model.

ARX788 inhibits tumor growth in HER2-positive and T-DM1–insensitive PDX models

PDX models provide an opportunity to test therapeutics in models with increased translational relevance. First, we directly compared activity of ARX788 and T-DM1 in two HER2-positive (IHC3+) breast cancer PDX models. In the MAXF1162 PDX model, mice (n = 10/group) treated with a single injection of ARX788 at 1 or 3 mg/kg resulted in significant, dose-dependent tumor killing with regression observed at the higher dose. However, treatment with 3 mg/kg T-DM1 led to significantly less activity than 3 mg/kg ARX788, and comparable activity with 1 mg/kg ARX788 (**Fig. 4A**).

Similarly, in the T226 PDX model, mice (n = 10/group) were administered a single injection of 1 or 3 mg/kg ARX788, 3 mg/kg T-DM1, or vehicle. The 3 mg/kg ARX788 significantly inhibited tumor growth, whereas treatment with the same dose of T-DM1 was ineffective (**Fig. 4B**). These results established significant antitumor activity of ARX788 in HER2-positive and T-DM1–insensitive breast cancer PDX models.

ARX788 efficacy in HER2-low expression breast cancer PDX models

To explore the potential to treat tumors with lower HER2 expression, we evaluated ARX788 activity in eight breast cancer PDX models (GenenDesign) with varying HER2 expression levels. HER2 expression in each PDX model was verified by IHC and FISH staining (**Fig. 4C** and **D**). Tumors stained IHC3+ or IHC2+/FISH positive (pos) were considered HER2 positive, and tumors stained IHC2+/FISH negative (neg) or IHC1+ were classified as HER2 low.

A single dose of 3 mg/kg ARX788 resulted in statistically significant TGI versus vehicle in four of six (67%) HER2-positive and in two of two (100%) HER2-low models (**Table 2**). This initial dataset showed significant ARX788 activity in both HER2-positive (IHC3+) and HER2-low (IHC2+/FISH neg) breast cancer PDX models.

Published OnlineFirst July 15, 2020; DOI: 10.1158/1535-7163.MCT-19-1004

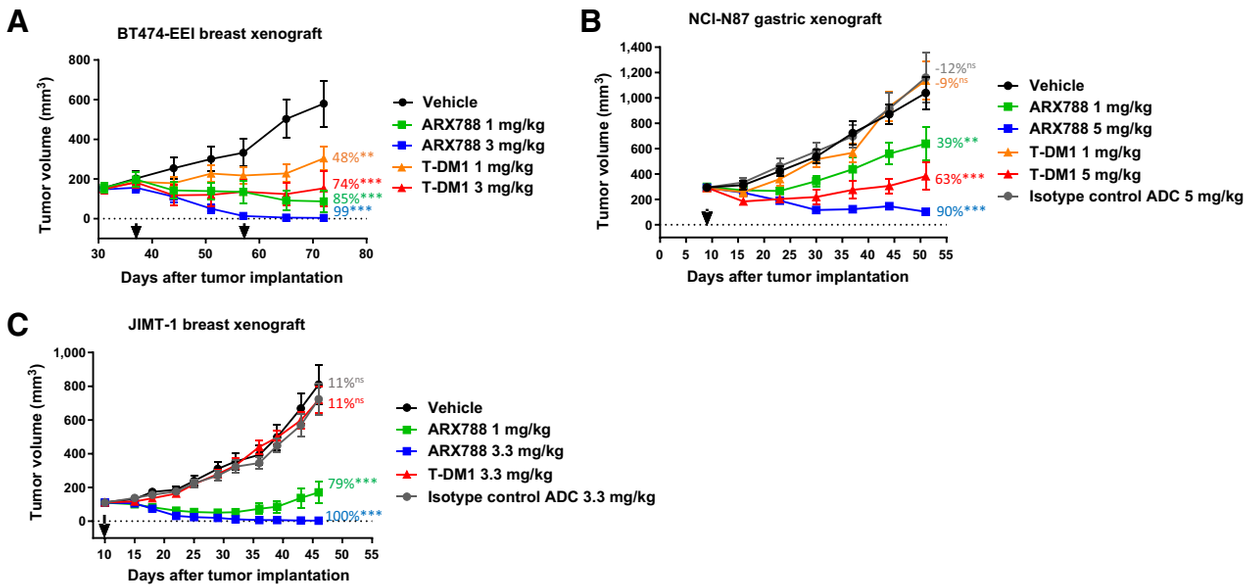

Figure 3.

In vivo efficacy of ARX788, T-DM1, and isotype control ADC in cell line–derived breast and gastric xenograft models with high HER2 expression, BT474-EEI (**A**) and NCI-N87 (**B**), and a breast xenograft model with lower HER2 expression, JIMT-1 (**C**). Mice ($n = 8$–10/group) were dosed intravenously once or twice (black arrows) with vehicle or ADCs, and mean tumor volumes (±SEM) are shown. % TGI and statistical significance ($P < 0.05$) versus vehicle were evaluated for each treatment group (*, $P < 0.05$; **, $P < 0.01$; ***, $P < 0.001$; ns, not significant).

Single and fractionated doses of ARX788 demonstrate activity in gastric PDX models

Next, we evaluated ARX788 activity in gastric cancer PDX models with HER2 status confirmed by IHC and FISH testing (**Fig. 4C** and **D**). A single 3 or 10 mg/kg dose of ARX788 resulted in significant TGI in three of four (75%) or four of four (100%) HER2-positive (IHC3+/FISH pos) models, respectively (**Table 3**).

The dose regimen was also modified to evaluate fractionated doses of 1 or 3 mg/kg ARX788 administered every 11 days for three total doses in eight gastric cancer PDX models. Multiple dose administration of ARX788 at 1 or 3 mg/kg significantly inhibited tumor growth in four of four (100%) HER2-positive and in three of four (75%) HER2-low gastric PDX models (**Table 3**). Interestingly, treatment with 3 mg/kg ARX788 caused complete tumor regression in PDX model STO #179, which stained as IHC1+/FISH neg.

Overall, the PDX studies provided evidence for ARX788 activity in: (i) HER2-positive tumors insensitive to T-DM1, (ii) breast and gastric tumors classified as HER2-positive or HER2-low (IHC2+/FISH neg or IHC1+) expression, and (iii) gastric tumors when administered at either a single high dose or as fractionated doses. A subset of the PDX model data is shown in Supplementary Fig. S3.

Discussion

First-generation ADCs are heterogeneous mixtures and have generally exhibited a narrow therapeutic window due to high toxicity and suboptimal efficacy. These ADCs primarily used random lysine or cysteine conjugation technology, which leads to heterogeneous populations with a varied number of drugs conjugated at different positions. Each population possesses different biophysical, *in vitro*, and *in vivo* properties (19). In addition, these conjugation chemistry and linker technologies can lead to deconjugation of the drug-linker or premature cleavage of the linker in systemic circulation (13, 24–26), thereby conferring off-target toxicity, as well as limiting the efficacy of the ADC. Safety issues such as neutropenia, peripheral neuropathy, and thrombocytopenia are commonly observed toxicities likely due to the premature release of drugs (26–28).

To address issues encountered by first-generation ADCs, we designed ARX788 for homogeneity and chemical stability, utilizing Ambrx's site-specific oxime conjugation technology and a noncleavable linker design. The Ambrx platform technology has advantages over other site-specific conjugation technologies such as the ability to incorporate nonnatural amino acid, pAF, at most sites within an antibody for conjugation, enabling incorporation of irreversible conjugation chemistries orthogonal to natural amino acids, and exploration of structure–activity relationship to optimize ADCs. A comprehensive comparison of the Ambrx Technology versus other site-specific conjugation technologies is discussed elsewhere (29).

ARX788 employs a highly potent hydrophilic payload with limited cell permeability to further improve the activity and safety profile, effectively widening the therapeutic window. Some ADC technologies have taken a different approach by attaching membrane-permeable payloads to elicit bystander killing on neighboring tumor cells that do not express target antigen (30–33). Permeable payloads can confer bystander activity in heterogeneous tumors, but may also result in increased off-target toxicity to normal tissues.

The hydrophilicity of the ARX788 PEG linker should render AS269 a poor substrate for MDR efflux pumps. Indeed, Kovtun and colleagues have reported PEG-linked ADCs were more effective than SMCC-linked ADCs in killing MDR-positive tumors (34). Takegawa and colleagues observed upregulation of MDR pumps in T-DM1–resistant cell lines, which were effectively targeted by Enhertu, reportedly not a strong MDR substrate (35).

When compared with T-DM1, ARX788 generally showed stronger *in vitro* and *in vivo* activity, particularly in the tumors with lower HER2 expression levels. Possible explanations for the differentiated activity

Published OnlineFirst July 15, 2020; DOI: 10.1158/1535-7163.MCT-19-1004

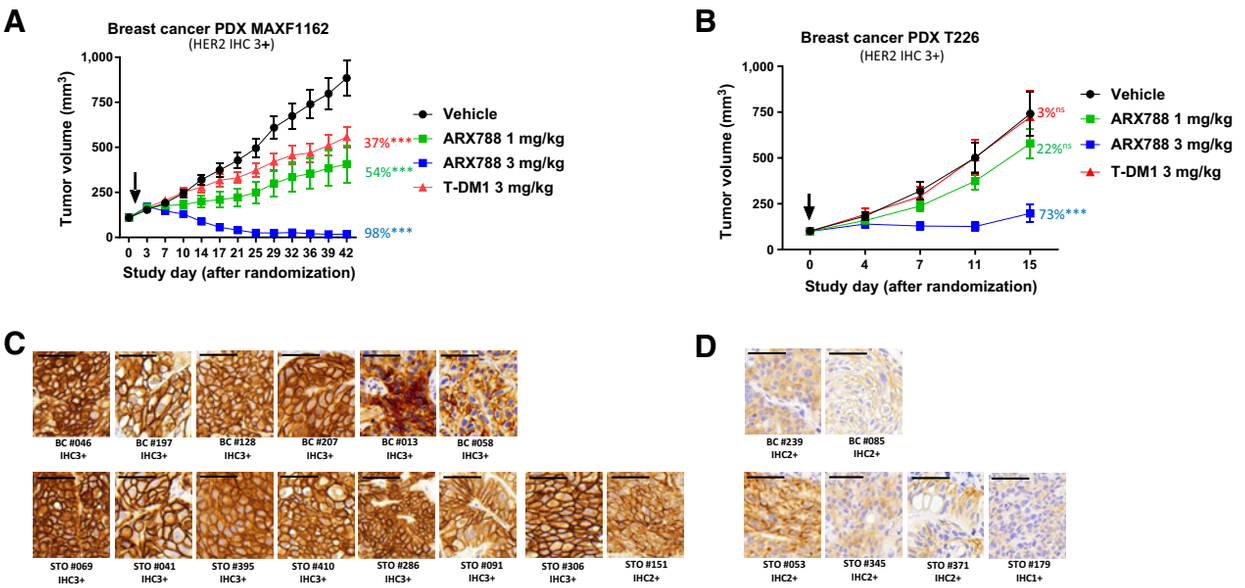

Figure 4.

ARX788 and T-DM1 activity in breast cancer PDX models, and IHC staining results for breast and gastric PDX models. Tumor growth curves for HER2 IHC3+ breast cancer PDX models, MAXF1162 (**A**) and T226 (**B**), after single dose administration (black arrows) of vehicle or ADCs are shown as mean tumor volume (± SEM). % TGI and statistical significance ($P < 0.05$) versus vehicle are listed for each treatment group ($n = 10$ mice/group). HER2 IHC staining (magnification, 40×; scale bar, 50 μm in top left corner) of GenenDesign PDX models arranged in HER2-positive (**C**) and HER2-low expression (**D**) groups (*, $P < 0.05$; **, $P < 0.01$; ***, $P < 0.001$; ns, not significant).

of ARX788 are the payload released by intracellular processing of ARX788 may have a slightly different mechanism of action, higher potency, or accumulates more efficiently intracellularly than the lys-MCC-DM1 payload released from T-DM1 (36).

Because of its stable linker and oxime conjugation, ARX788 exhibits higher serum stability and a longer half-life than T-DM1. In a mouse pharmacokinetic study, ARX788 remained intact as a DAR2 ADC throughout the study, with a long terminal half-life of 12.5 days. In contrast, T-DM1 was unstable with a terminal half-life of 5.7 days in the ADC assay and 11 days in the total antibody assay (36). In addition, ARX788 shows a similar half-life and exposure as the unconjugated anti-HER2 mAb, whereas ADCs with random conjugation of relatively hydrophobic payloads tend to exhibit lower exposure and a shorter half-life than their unconjugated antibody (14, 37).

ARX788 showed strong, HER2-dependent activity in cancer cell lines expressing ≥60,000 or 100,000 HER2 receptors (IHC1+ or 2+) and was inactive in breast cancer cell lines and normal cardiomyocytes expressing ≤20,000 HER2 receptors (IHC0). Similarly, ARX788

Table 2. Breast cancer PDX models.

BC PDX model	HER2 status	Route/schedule	Dose (mg/kg)	%TGI	*P*
BC #046	HER2 pos (IHC3+/FISH pos)	i.v.: QD × 1	1	**84**	<0.05
			3	**99**	<0.05
BC #013	HER2 pos (IHC3+/FISH pos)	i.v.: QD × 1	1	**85**	<0.05
			3	**92**	<0.05
BC #197	HER2 pos (IHC3+/FISH pos)	i.v.: QD × 1	1	66	<0.05
			3	**91**	<0.05
BC #128	HER2 pos (IHC3+/FISH pos)	i.v.: QD × 1	1	−25	ns
			3	47	<0.05
BC #207	HER2 pos (IHC3+/FISH pos)	i.v.: QD × 1	1	18	ns
			3	20	ns
BC #058	HER2 pos (IHC3+/FISH neg)	i.v.: QD × 1	1	20	ns
			3	38	ns
BC #239	HER2 low (IHC2+/FISH neg)	i.v.: QD × 1	1	68	<0.05
			3	**87**	<0.05
BC #085	HER2 low (IHC2+/FISH neg)	i.v.: QD × 1	1	42	<0.05
			3	57	<0.05

Note: Bold text indicates tumor regression (% TGI > 80).
Abbreviations: BC, breast cancer; i.v., intravenous; ns, not significant; QD × 1, every day.

Published OnlineFirst July 15, 2020; DOI: 10.1158/1535-7163.MCT-19-1004

Table 3. Gastric cancer PDX models.

GC PDX model	HER2 status	Route/schedule	Dose (mg/kg)	% TGI	*P*
STO #069	HER2 pos (IHC3+/FISH pos)	i.v.: QD × 1	3	35	<0.05
			10	**100**	<0.05
STO #041	HER2 pos (IHC3+/FISH pos)	i.v.: QD × 1	3	43	<0.05
			10	**96**	<0.05
STO #395	HER2 pos (IHC3+/FISH pos)	i.v.: QD × 1	3	**81**	<0.05
			10	**93**	<0.05
STO #410	HER2 pos (IHC3+/FISH pos)	i.v.: QD × 1	3	14	ns
			10	**95**	<0.05
STO #151	HER2 pos (IHC2+/FISH pos)	i.v.: Q11D × 3	1	**97**	<0.05
			3	**100**	<0.05
STO #306	HER2 pos (IHC3+/FISH pos)	i.v.: Q11D × 3	1	**86**	<0.05
			3	**99**	<0.05
STO #286	HER2 pos (IHC3+/FISH pos)	i.v.: Q11D × 3	1	**86**	<0.05
			3	**96**	<0.05
STO #091	HER2 pos (IHC3+/FISH pos)	i.v.: Q11D × 3	1	50	<0.05
			3	58	<0.05
STO #179	HER2 low (IHC1+/FISH neg)	i.v.: Q11D × 3	1	**84**	<0.05
			3	**100**	<0.05
STO #053	HER2 low (IHC2+/FISH neg)	i.v.: Q11D × 3	1	47	<0.05
			3	**82**	<0.05
STO #345	HER2 low (IHC2+/FISH neg)	i.v.: Q11D × 3	1	34	<0.05
			3	59	<0.05
STO #371	HER2 low (IHC2+/FISH neg)	i.v.: Q11D × 3	1	25	ns
			3	19	ns

Note: Bold text indicates tumor regression (% TGI >80).
Abbreviations: GC, gastric cancer; i.v., intravenous; ns, not significant; QD × 1, every day; Q11D × 3, every 11 days.

inhibited tumor growth in xenograft models and in HER2-positive or HER2-low (IHC2+/FISH neg or IHC1+) PDX models, when administered at a single dose or as fractionated doses.

The dose fractionation strategy has been tested in clinic for ADCs, especially for unstable ADCs, to decrease toxicity while maintaining efficacy (38, 39). Mylotarg was reapproved by the FDA when investigators demonstrated dose fractionation (3 mg/m^2 on days 1, 4, and 7) showed similar activity as a higher dose (9 mg/m^2 on days 1 and 15) but with much lower toxicity (3). Although not directly compared with a single dose in the same PDX model, dose fractionation of ARX788 inhibited tumor growth to a comparable level and suggests optimization of ARX788 dose could further decrease potential toxicity in clinical testing.

Interestingly, ARX788, which is designed without bystander effect, caused tumor regression in a HER2 IHC1+/FISH neg PDX model. Review of the IHC stain results showed faint, yet relatively homogeneous, staining of the tumor cell population. Consistent with *in vitro* data, it is possible the HER2 expression level present on the IHC1+ tumor cells enabled ARX788 to deliver a sufficient quantity of payload to kill tumor cells. This finding highlights the potential of ARX788 to be efficacious in the HER2 IHC1+/FISH neg patient population.

ARX788 was designed to address *in vivo* instability issues observed with first-generation ADCs, however, it may lead to nonspecific toxicities as a result of its prolonged circulating half-life due to nonspecific uptake by normal tissue or binding to non-HER2 targets by components of the ADC, such as Fc, linker, and drug. The nonspecific or off-target toxicity of ADCs is complex and not completely understood. A recent publication reported T-DM1 bound to cell surface CKAP5 via DM1 and damaged hepatocytes, but ADCs with auristatin payloads did not bind CKAP5 or exert this effect (40). ARX788 treatment was well-tolerated in all efficacy studies, with no significant body weight loss observed in any animals. Rat and cynomolgus toxicity studies have been conducted to evaluate the target-independent and target-dependent toxicity profiles of ARX788. These data, and additional nonclinical studies, are discussed in a separate manuscript (submitted).

In conclusion, we have developed ARX788, a homogeneous, highly stable, and potent next-generation site-specific anti-HER2 ADC. ARX788 exhibited enhanced pharmacokinetics and significant *in vivo* efficacy against HER2-positive tumors, HER2-low expression tumors, and T-DM1–resistant tumors. The data suggest ARX788 may be an effective treatment for cancer patients with HER2-low (IHC2+/FISH neg or IHC1+) tumors, a population with high unmet medical need as they currently are ineligible to receive HER2-targeted therapy. The promising preclinical data support advancing ARX788 into clinical testing. ARX788 is currently in phase I clinical trials for breast and gastric cancers in the United States, Australia, New Zealand, and China.

Disclosure of Potential Conflicts of Interest

L. Skidmore reports a patent for US9796754 issued. S.L. Biroc reports a patent US9796754 issued. R. Marsden reports a patent US9796754 issued. I. Lopez reports a patent for US9796754 issued. No potential conflicts of interest were disclosed by the other authors.

Authors' Contributions

L. Skidmore: Conceptualization, formal analysis, supervision, investigation, visualization, methodology, writing-original draft, project administration, writing-review and editing. **S. Sakamuri:** Conceptualization, supervision, writing-original draft, writing-review and editing. **N.A. Knudsen:** Formal analysis, investigation, visualization, methodology, writing-review and editing. **A.G. Hewet:** Formal analysis, investigation, visualization, methodology, writing-review and editing. **S. Milutinovic:** Formal analysis, visualization, methodology, project administration, writing-review and editing. **W. Barkho:** Formal analysis, visualization, project administration, writing-review and editing. **S.L. Biroc:** Formal analysis, supervision, visualization, methodology, project administration, writing-review and editing. **J. Kirtley:**

Published OnlineFirst July 15, 2020; DOI: 10.1158/1535-7163.MCT-19-1004

Investigation, methodology, writing-review and editing. **R. Marsden:** Formal analysis, investigation, visualization, methodology, project administration, writing-review and editing. **K. Storey:** Formal analysis, investigation, visualization, methodology, writing-review and editing. **I. Lopez:** Formal analysis, investigation, visualization, methodology, writing-review and editing. **W. Yu:** Formal analysis, visualization, methodology, project administration, writing-review and editing. **S.-Y. Fang:** Formal analysis, investigation, visualization, methodology, writing-review and editing. **S. Yao:** Supervision, writing-review and editing. **Y. Gu:** Conceptualization, supervision, methodology, project administration, writing-review and editing. **F. Tian:** Conceptualization, supervision, methodology, project administration, writing-review and editing.

Acknowledgments

We would like to thank Shawn Zhang for helpful comments on the article, and Claire Kao for performing the RP-HPLC analytical experiments.

The costs of publication of this article were defrayed in part by the payment of page charges. This article must therefore be hereby marked *advertisement* in accordance with 18 U.S.C. Section 1734 solely to indicate this fact.

Received October 22, 2019; revised April 16, 2020; accepted July 8, 2020; published first July 15, 2020.

References

1. de Claro RA, McGinn K, Kwitkowski V, Bullock J, Khandelwal A, Habtemariam B, et al. U.S. Food and Drug Administration approval summary: brentuximab vedotin for the treatment of relapsed Hodgkin lymphoma or relapsed systemic anaplastic large-cell lymphoma. Clin Cancer Res 2012;18:5845–9.
2. Verma S, Miles D, Gianni L, Krop IE, Welslau M, Baselga J, et al. Trastuzumab emtansine for HER2-positive advanced breast cancer. N Engl J Med 2012;367:1783–91.
3. Norsworthy KJ, Ko CW, Lee JE, Liu J, John CS, Przepiorka D, et al. FDA approval summary: mylotarg for treatment of patients with relapsed or refractory CD33-positive acute myeloid leukemia. Oncologist 2018;23:1103–8.
4. Kantarjian HM, DeAngelo DJ, Stelljes M, Liedtke M, Stock W, Gökbuget N, et al. Inotuzumab Ozogamicin versus standard of care in relapsed or refractory acute lymphoblastic leukemia: final report and long-term survival follow-up from the randomized, phase 3 INO-VATE study. Cancer 2019;125:2474–87.
5. Sehn LH, Herrera AF, Matasar MJ, Kamdar M, McMillan AK, Kim TM, et al. Addition of polatuzumab vedotin to bendamustine and rituximab (BR) improves outcomes in transplant-ineligible patients with relapsed/refractory (R/R) diffuse large B-cell lymphoma (DLBCL) versus BR alone: results from a randomized phase 2 study. Blood 2017;130:2821.
6. Rosenberg JE, O'Donnell PH, Balar AV, McGregor BA, Heath EI, Yu EY, et al. Pivotal trial of enfortumab vedotin in urothelial carcinoma after platinum and anti-programmed death 1/programmed death ligand 1 therapy. J Clin Oncol 2019;37:2592–600.
7. Modi S, Saura C, Yamashita T, Park YH, Kim S-B, Tamura K, et al. Trastuzumab deruxtecan in previously treated HER2-positive breast cancer. N Engl J Med 2020;382:610–21.
8. Waight AB, Bargsten K, Doronina S, Steinmetz MO, Sussman D, Prota AE, et al. Structural basis of microtubule destabilization by potent auristatin antimitotics. PLoS One 2016;11:e0160890.
9. Doronina SO, Mendelsohn BA, Bovee TD, Cerveny CG, Alley SC, Meyer DL, et al. Enhanced activity of monomethylauristatin F through monoclonal antibody delivery: effects of linker technology on efficacy and toxicity. Bioconjug Chem 2006;17:114–24.
10. Francisco JA, Cerveny CG, Meyer DL, Mixan BJ, Klussman K, Chace DF, et al. cAC10-vcMMAE, an anti-CD30–monomethyl auristatin E conjugate with potent and selective antitumor activity. Blood 2003;102:1458–65.
11. van der Lee MM, Groothuis PG, Ubink R, van der Vleuten MA, van Achterberg TA, Loosveld EM, et al. The preclinical profile of the duocarmycin-based HER2-targeting ADC SYD985 predicts for clinical benefit in low HER2-expressing breast cancers. Mol Cancer Ther 2015;14:692–703.
12. Li JY, Perry SR, Muniz-Medina V, Wang X, Wetzel LK, Rebelatto MC, et al. A biparatopic HER2-targeting antibody-drug conjugate induces tumor regression in primary models refractory to or ineligible for HER2-targeted therapy. Cancer Cell 2016;29:117–29.
13. Shen BQ, Xu K, Liu L, Raab H, Bhakta S, Kenrick M, et al. Conjugation site modulates the *in vivo* stability and therapeutic activity of antibody-drug conjugates. Nat Biotechnology 2012;30:184–9.
14. Lyon RP, Bovee TD, Doronina SO, Burke PJ, Hunter JH, Neff-LaFord HD, et al. Reducing hydrophobicity of homogeneous antibody-drug conjugates improves pharmacokinetics and therapeutic index. Nat Biotechnol 2015;33:733–5.
15. Lewis Phillips GD, Li G, Dugger DL, Crocker LM, Parsons KL, Mai E, et al. Targeting HER2-positive breast cancer with trastuzumab-DM1, an antibody-cytotoxic drug conjugate. Cancer Res 2008;68:9280–90.
16. Jeffrey SC, Burke PJ, Lyon RP, Meyer DW, Sussman D, Anderson M, et al. A potent anti-CD70 antibody-drug conjugate combining a dimeric pyrrolobenzodiazepine drug with site-specific conjugation technology. Bioconjug Chem 2013;24:1256–63.
17. Tian F, Lu Y, Manibusan A, Sellers A, Tran H, Sun Y, et al. A general approach to site-specific antibody drug conjugates. Proc Natl Acad Sci U S A 2014;111:1766–71.
18. Jackson D, Atkinson J, Guevara CI, Zhang C, Kery V, Moon SJ, et al. *In vitro* and *in vivo* evaluation of cysteine and site specific conjugated herceptin antibody-drug conjugates. PLoS One 2014;9:e83865.
19. Hamblett KJ, Senter PD, Chace DF, Sun MM, Lenox J, Cerveny CG, et al. Effects of drug loading on the antitumor activity of a monoclonal antibody drug conjugate. Clin Cancer Res 2004;10:7063–70.
20. Junutula JR, Flagella KM, Graham RA, Parsons KL, Ha E, Raab H, et al. Engineered thio-trastuzumab-DM1 conjugate with an improved therapeutic index to target human epidermal growth factor receptor 2-positive breast cancer. Clin Cancer Res 2010;16:4769–78.
21. Dennler P, Chiotellis A, Fischer E, Brégeon D, Belmant C, Gauthier L, et al. Transglutaminase-based chemo-enzymatic conjugation approach yields homogeneous antibody–drug conjugates. Bioconjug Chem 2014;25:569–78.
22. Beerli RR, Hell T, Merkel AS, Grawunder U. Sortase enzyme-mediated generation of site-specifically conjugated antibody drug conjugates with high *in vitro* and *in vivo* potency. PLoS ONE 2015;10:e0131177.
23. van Geel R, Wijdeven MA, Heesbeen R, Verkade JMM, Wasiel AA, van Berkel SS, et al. Chemoenzymatic conjugation of toxic payloads to the globally conserved N-glycan of native mAbs provides homogeneous and highly efficacious antibody-drug conjugates. Bioconjug Chem 2015;26:2233–42.
24. Alley SC, Benjamin DR, Jeffrey SC, Okeley NM, Meyer DL, Sanderson RJ, et al. Contribution of linker stability to the activities of anticancer immunoconjugates. Bioconjug Chem 2008;19:759–65.
25. Ponte JF, Sun X, Yoder NC, Fishkin N, Laleau R, Coccia J, et al. Understanding how the stability of the thiol-maleimide linkage impacts the pharmacokinetics of lysine-linked antibody–maytansinoid conjugates. Bioconjugate Chem 2016;27:1588–98.
26. Mahalingaiah PK, Ciurlionis R, Durbin KR, Yeager RL, Philip BK, Bawa B, et al. Potential mechanisms of target-independent uptake and toxicity of antibody-drug conjugates. Pharmacol Ther 2019;200:110–25.
27. Donaghy H.Effects of antibody, drug and linker on the preclinical and clinical toxicities of antibody-drug conjugates. mAbs 2016;8:659–71.
28. Zhao H, Gulesserian S, Malinao MC, Ganesan SK, Song J, Chang MS, et al. A potential mechanism for ADC-induced neutropenia: role of neutrophils in their own demise. Mol Cancer Ther 2017;16:1866–76.
29. Tian F, Jackson D, Bai Y. Site-specific antibody-drug conjugates. In: Damelin M, editor. Innovations for next-generation antibody-drug conjugates. cancer drug discovery and development. Cham, Switzerland: Humana Press; 2018. p. 241–65.
30. Okeley NM, Miyamoto JB, Zhang X, Sanderson RJ, Benjamin DR, Sievers EL, et al. Intracellular activation of SGN-35, a potent anti-CD30 antibody-drug conjugate. Clin Cancer Res 2010;16:888–97.
31. Li F, Emmerton KK, Jonas M, Zhang X, Miyamoto JB, Setter JR, et al. Intracellular released payload influences potency and bystander-killing effects of antibody-drug conjugates in preclinical models. Cancer Res 2016;76:2710–9.
32. Ogitani Y, Hagihara K, Oitate M, Naito H, Agatsuma T. Bystander killing effect of DS-8201a, a novel anti-human epidermal growth factor receptor 2 antibody–drug conjugate, in tumors with human epidermal growth factor receptor 2 heterogeneity. Cancer Sci 2016;107:1039–46.

33. Golfier S, Kopitz C, Kahnert A, Heisler I, Schatz CA, Stelte-Ludwig B, et al. Anetumab ravtansine: a novel mesothelin-targeting antibody-drug conjugate cures tumors with heterogeneous target expression favored by bystander effect. Mol Cancer Ther 2014;13:1537–48.
34. Kovtun YV, Audette CA, Mayo MF, Jones GE, Doherty H, Maloney EK, et al. Antibody-maytansinoid conjugates designed to bypass multidrug resistance. Cancer Res 2010;70:2528–37.
35. Takegawa N, Nonagase Y, Yonesaka K, Sakai K, Maenishi O, Ogitani Y, et al. DS-8201a, a new HER2-targeting antibody-drug conjugate incorporating a novel DNA topoisomerase I inhibitor, overcomes HER2-positive gastric cancer T-DM1 resistance. Int J Cancer 2017;141:1682–9.
36. Erickson HK, Lewis Phillips GD, Leipold DD, Provenzano CA, Mai E, Johnson HA, et al. The effect of different linkers on target cell catabolism and pharmacokinetics/pharmacodynamics of trastuzumab maytansinoid conjugates. Mol Cancer Ther 2012;11:1133–42.
37. Boswell CA, Mundo EE, Zhang C, Bumbaca D, Valle NR, Kozak KR, et al. Impact of drug conjugation on pharmacokinetics and tissue distribution of anti-STEAP1 antibody–drug conjugates in rats. Bioconjug Chem 2011;22:1994–2004.
38. Hinrichs MJM, Ryan PM, Zheng B, Afif-Rider S, Yu XQ, Gunsior M, et al. Fractionated dosing improves preclinical therapeutic index of pyrrolobenzodiazepine-containing antibody drug conjugates. Clin Cancer Res 2017;23:5858–68.
39. Ribrag V, Dupuis J, Tilly H, Morschhauser F, Laine F, Houot R, et al. A dose-escalation study of SAR3419, an anti-CD19 antibody maytansinoid conjugate, administered by intravenous infusion once weekly in patients with relapsed/refractory B-cell non-Hodgkin lymphoma. Clin Cancer Res 2014;20:213–20.
40. Endo Y, Takeda K, Mohan N, Shen Y, Jiang J, Rotstein D, et al. Payload of T-DM1 binds to cell surface cytoskeleton-associated protein 5 to mediate cytotoxicity of hepatocytes. Oncotarget 2018;9:37200–15.

Published OnlineFirst July 15, 2020; DOI: 10.1158/1535-7163.MCT-19-1004

Molecular Cancer Therapeutics

ARX788, a Site-specific Anti-HER2 Antibody–Drug Conjugate, Demonstrates Potent and Selective Activity in HER2-low and T-DM1 –resistant Breast and Gastric Cancers

Lillian Skidmore, Sukumar Sakamuri, Nick A. Knudsen, et al.

Mol Cancer Ther 2020;19:1833-1843. Published OnlineFirst July 15, 2020.